Enhanced activation of an amino-terminally truncated isoform of the voltage-gated proton channel HVCN1 enriched in malignant B cells

Elayne Hondares[a], Mark Adrian Brown[a], Boris Musset[b], Deri Morgan[c], Vladimir V. Cherny[c], Christina Taubert[a,1], Mandeep K. Bhamrah[d,2], David Coe[e], Federica Marelli-Berg[e], John G. Gribben[f], Martin J. S. Dyer[g], Thomas E. DeCoursey[c,3], and Melania Capasso[a,3]

[a]Centre for Cancer and Inflammation, Barts Cancer Institute, Queen Mary University of London, London EC1M 6BQ, United Kingdom; [b]ICS-4 Forschungszentrum Jülich, 52425 Jülich, Germany; [c]Department of Molecular Biophysics and Physiology, Rush University, Chicago, IL 60612; [d]Medical Research Council Toxicology Unit, Leicester LE1 9HN, United Kingdom; [e]Centre for Biochemical Pharmacology, William Harvey Research Institute, Queen Mary University of London, London EC1M 6BQ, United Kingdom; [f]Centre for Haemato-Oncology, Barts Cancer Institute, Queen Mary University of London, London EC1M 6BQ, United Kingdom; and [g]Ernest and Helen Scott Haematological Research Institute, University of Leicester, Leicester LE1 9HN, United Kingdom

Edited* by Michael D. Cahalan, University of California, Irvine, CA, and approved October 31, 2014 (received for review June 19, 2014)

HVCN1 (Hydrogen voltage-gated channel 1) is the only mammalian voltage-gated proton channel. In human B lymphocytes, HVCN1 associates with the B-cell receptor (BCR) and is required for optimal BCR signaling and redox control. HVCN1 is expressed in malignant B cells that rely on BCR signaling, such as chronic lymphocytic leukemia (CLL) cells. However, little is known about its regulation in these cells. We found that HVCN1 was expressed in B cells as two protein isoforms. The shorter isoform ($HVCN1_S$) was enriched in B cells from a cohort of 76 CLL patients. When overexpressed in a B-cell lymphoma line, $HVCN1_S$ responded more profoundly to protein kinase C-dependent phosphorylation. This more potent enhanced gating response was mediated by increased phosphorylation of the same residue responsible for enhanced gating in $HVCN1_L$, Thr^{29}. Furthermore, the association of $HVCN1_S$ with the BCR was weaker, which resulted in its diminished internalization upon BCR stimulation. Finally, $HVCN1_S$ conferred a proliferative and migratory advantage as well as enhanced BCR-dependent signaling. Overall, our data show for the first time, to our knowledge, the existence of a shorter isoform of HVCN1 with enhanced gating that is specifically enriched in malignant B cells. The properties of $HVCN1_S$ suggest that it may contribute to the pathogenesis of BCR-dependent B-cell malignancies.

proton currents | chronic lymphocytic leukemia | Hv1 | gating kinetics | phosphorylation

The voltage-gated proton channel HVCN1 (or H_V1 or VSOP) is a small protein that conducts protons across membranes selectively (1, 2) and in a regulated manner. Previously, we described its function in B lymphocytes, where proton channels sustain B-cell receptor (BCR) signaling via regulation of reactive oxygen species production by the NADPH oxidase enzyme complex (3). In addition, we found HVCN1 to be directly associated with the BCR. Upon receptor stimulation, the BCR and HVCN1 were cointernalized to late endosomal/lysosomal organelles called "MIICs," or MHC class II-containing compartments, where antigens bound to the BCR are digested into small peptides and loaded onto MHC class II molecules for presentation to T cells (3).

HVCN1 is expressed not only by normal but also by malignant B cells, such as those in chronic lymphocytic leukemia (CLL) (3). CLL cells are characterized by their reliance on BCR signaling for survival and growth (4), so it is possible that they maintain or upregulate HVCN1 expression to sustain their growth. Other tumor cells, such as those in breast (5) and colorectal cancer (6), have been found to rely on HVCN1 for survival. In these tumor cells, proton channels prevent excessive acidification of the cytoplasm and allow increased cell migration. In malignant B cells, HVCN1 may regulate intracellular pH and at the same time sustain BCR signaling. However, its precise roles remain to be elucidated.

We show here that CLL cells and other B-cell lines specifically express higher levels of a shorter isoform of HVCN1, $HVCN1_S$. We identified the existence of two distinct isoforms of relatively similar size when immunoblotting B-cell lysates with an HVCN1-specific antibody (3). $HVCN1_S$ is only weakly expressed in normal B cells, and in light of its apparent upregulation in tumor cells, we set out to characterize its function. We show that $HVCN1_S$ responds more strongly to phosphorylation by protein kinase C (PKC) and identify the phosphorylation site. We provide evidence that $HVCN1_S$ in B cells is preferentially expressed at the plasma membrane, even upon BCR stimulation and subsequent internalization, due to a weaker association with the BCR. Finally, we show that $HVCN1_S$ expression results in stronger BCR signaling, increased proliferation, and augmented chemokine-dependent migration. Overall, our data indicate that $HVCN1_S$ is an alternative protein isoform that mediates stronger currents upon PKC phosphorylation, is more highly expressed at the plasma membrane, and can confer a growth advantage to malignant B cells.

Significance

B lymphocytes are crucial cells in immune responses. Their activity is regulated by signaling pathways involving reactive oxygen species (ROS). Voltage-gated proton channels modulate B-cell responses by facilitating production of ROS. Here we compare the full-length proton channel $HVCN1_L$ with a shorter protein isoform, $HVCN1_S$, which lacks the first 20 amino acids. Cells with $HVCN1_S$ display enhanced proton currents upon stimulation. In addition, $HVCN1_S$ is internalized to a lesser extent by interactions with the B-cell receptor, resulting in greater plasma membrane expression. Finally, $HVCN1_S$ expression results in greater proliferation and migration. Compared with normal B lymphocytes, $HVCN1_S$ expression is higher in B-cell lines and in B cells from patients with chronic lymphocytic leukemia, where it may contribute to disease pathogenesis.

Author contributions: F.M.-B., T.E.D., and M.C. designed research; E.H., M.A.B., B.M., D.M., V.V.C., C.T., M.K.B., D.C., and M.C. performed research; J.G.G. and M.J.S.D. contributed new reagents/analytic tools; E.H., M.A.B., B.M., D.M., V.V.C., C.T., T.E.D., and M.C. analyzed data; and E.H., M.A.B., M.J.S.D., T.E.D., and M.C. wrote the paper.

The authors declare no conflict of interest.

*This Direct Submission article had a prearranged editor.

[1]Present address: Medical Research Council National Institute for Medical Research, London NW7 1AA, United Kingdom.

[2]Present address: Cancer Research Technology, London EC1V 4AD, United Kingdom.

[3]To whom correspondence may be addressed. Email: tdecours@rush.edu or m.capasso@qmul.ac.uk.

This article contains supporting information online at www.pnas.org/lookup/suppl/doi:10.1073/pnas.1411390111/-/DCSupplemental.

Results

Identification of an HVCN1 Isoform Enriched in Malignant B Cells. We investigated HVCN1 expression in a panel of B-cell lines and noted the presence of two bands of similar molecular weight. Some cell lines appeared to express more of the shorter isoform, whereas the Burkitt cell line Raji expressed it exclusively (Fig. 1*A*, *Left*). Peripheral blood B cells expressed this short isoform (here called $HVCN1_S$) at much lower levels compared with CLL cells (Fig. 1*A*, *Center* and *Right*).

When we started this study, the GenBank database reported only one viable splicing variant for human HVCN1 (*SI Appendix*, Fig. S1, variant 1). Given the presence of an ATG 60 base pairs (bp) downstream from the first ATG, we set out to investigate if a shorter isoform could be the result of translation from this alternative start site. To this end, we expressed recombinant HVCN1 Long ($HVCN1_L$) in an in vitro translation assay (Fig. 1*B*, *Left*). We then mutated the first ATG to TTG, which resulted in significantly reduced translation from this codon (Fig. 1*B*, *Center*). A shorter protein was expressed from the mutated plasmid (Fig. 1*B*, *Center*) when expressed in whole cells also (Fig. 1*C*, *Right*), indicating that the second ATG functioned as a start codon.

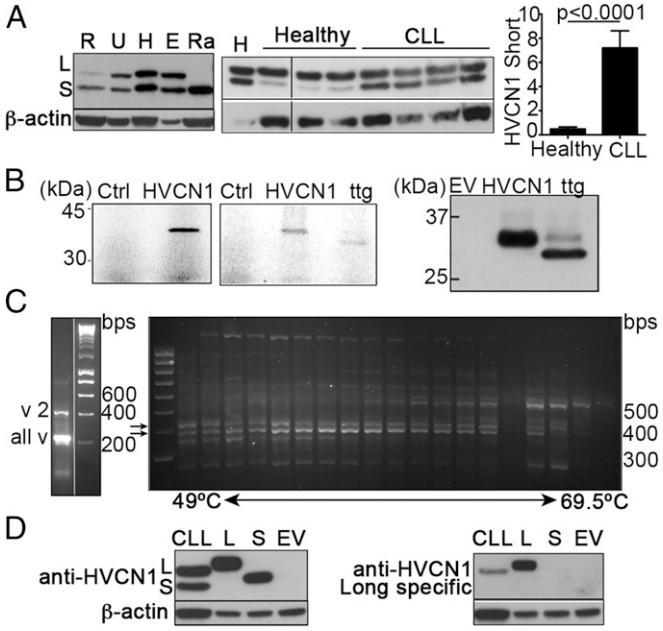

Fig. 1. $HVCN1_S$ is an alternative isoform of the voltage-gated proton channel HVCN1 enriched in malignant B cells. (*A*, *Left* and *Center*) Immunoblots showing expression of two isoforms of HVCN1, $HVCN1_L$ ("L"), and $HVCN1_S$ ("S") in B-cell lines, primary B cells, and CLL samples. R (RI1), U (U2932), and H (HBL1) are diffuse large B-cell lymphoma cell lines; E (EJM) is a multiple myeloma cell line, and Ra (RAJI) is a Burkitt lymphoma cell line. (*Right*) Densitometry analysis of protein expression of $HVCN1_S$ in B cells from healthy donors ($n = 7$) and CLL patients ($n = 76$). Protein expression levels as determined by Western blot, relative to loading control (β-actin or α-tubulin) and normalized to a positive control used across different blots (cell line HBL1). Statistical analysis carried out with Mann–Whitney *U* test. (*B*, *Left* and *Center*) In vitro transcription-translation assays with recombinant $HVCN1_L$ and mutated $ttgHVCN1_L$. (*Right*) Expression of $ttgHVCN1_L$ transduced in LK35.2 cells. (*C*) PCR on HBL1 mRNA to identify the three mRNA sequences reported for human HVCN1 (*SI Appendix*, Fig. S1). (*Left*) Duplex PCR with primers designed for mRNA variant 2, which amplifies a band of 432 bp, and primers recognizing all variants (228 bp). (*Right*) PCR performed with different annealing temperatures with primers designed to recognize HVCN1 mRNA variants 1 and 3. The expected bands for isoforms 1 and 3 are 433 and 393 bp, indicated by arrows. (*D*) Immunoblots of a CLL sample and LK35.2 cells overexpressing $HVCN1_L$ and $HVCN1_S$ with an anti-HVCN1 that recognizes residues 26–46 (*Left*) and residues 1–20 ($HVCN1_L$-specific, *Right*).

More recently, three splicing variants for human HVCN1 have been reported (*SI Appendix*, Fig. S1). Variant 1 and 2 differ in the use of alternative 5′-untranslated regions (UTRs) but code for the same full-length HVCN1 protein, whereas variant 3 uses the same 5′-UTR as variant 1 but it does not possess the first coding exon. Therefore, variant 3 lacks the first ATG and consequently translation can start only from the second ATG 60 bp downstream. To test the existence of the three mRNA variants, we designed specific PCR primers and tested them with mRNA from the cell line HBL1. We used the same reverse primer and specific forward primers for variants 1/3 and 2, annealing on their respective 5′-UTRs. To distinguish variants 1 and 3, we relied on differences in the band size of the amplified PCR product (433 for variant 1 and 393 for variant 3). As Fig. 1*C*, *Left*, shows, the PCR with primers for variant 2 and all variants produced bands of the expected sizes. For variants 1 and 3, we ran a gradient PCR (Fig. 1*C*, *Right*), which showed the expected bands of 433 and 393 bp (Fig. 1*C*, arrows). Overall, our results indicate the existence of three distinct mRNA variants and therefore suggest that $HVCN1_S$ is the result of alternative mRNA splicing, which produces a protein identical to the long isoform but lacking the first 20 amino acids.

To confirm the nature of this shorter isoform, we raised an antibody toward the first 20 amino acids of HVCN1, which should recognize the long isoform only. Our original anti-HVCN1 antibody, which recognizes a region in the N terminus closer to the first transmembrane domain (amino acids 26–46), detected both isoforms in CLL cells (Fig. 1*D*, *Left*). Also, recombinant $HVCN1_L$ and $HVCN1_S$ were both detected. In contrast, an immunoblot with the anti-$HVCN1_L$–specific antibody detected only the long isoform, both recombinant and endogenously expressed (Fig. 1*D*, *Right*). These results confirmed that the shorter isoform of HVCN1 is a protein with a shorter N terminus domain, lacking the first 20 amino acids.

Both Isoforms Are Voltage-Gated Proton Channels. Biophysical properties of $HVCN1_L$ and $HVCN1_S$ were compared in transduced LK-35.2 cells using the whole-cell voltage-clamp configuration over a wide range of pH. The H^+ currents generated by the two isoforms appeared generally similar. *SI Appendix*, Fig. S2*A*, confirms that both isoforms were proton selective because the reversal potential for current (V_{rev}) was close to the Nernst potential for H^+ (E_H). This result is expected because the selectivity filter is in the middle of the S1 transmembrane helix (1), far from the N terminus where the two isoforms differ.

A unique property of all known voltage-gated proton channels crucial to their function is ΔpH-dependent gating (2, 7). The position of the proton conductance–voltage (g_H–V) relationship depends strongly on both pH_o and pH_i, with the consequence that the channel opens only when there is an outward electrochemical gradient, and the open channel will extrude H^+ from the cell. $HVCN1_L$ and $HVCN1_S$ exhibited similar ΔpH-dependent gating, both activating at potentials about 10 mV positive to V_{rev} at symmetrical pH (*SI Appendix*, Fig. S2*B*).

To compare gating kinetics, we used the perforated-patch voltage-clamp method, a more physiological configuration that preserves cytoplasmic contents. Comparison of the gating kinetics of $HVCN1_L$ and $HVCN1_S$ in unstimulated LK-35.2 cells (*SI Appendix*, Table S1) reveals that $HVCN1_S$ channels opened more slowly, with a time constant of current turn-on, τ_{act}, more than double that of $HVCN1_L$. Closing kinetics (τ_{tail}) and the position of the g_H-V relationship did not differ significantly.

$HVCN1_S$ Responds More Strongly to PKC-Dependent Phosphorylation. Proton currents in phagocytes and other cells are greatly augmented by phosphorylation of the channel by PKC (8). The enhanced gating response is stimulated effectively by the PKC activator PMA (phorbol myristate acetate) and is best studied

PHYSIOLOGY

using the perforated-patch configuration that preserves intracellular signaling pathways (9). Fig. 2 illustrates families of proton currents in cells expressing $HVCN1_L$ and $HVCN1_S$ before and after PMA stimulation. In response to PMA, the currents turn on more rapidly and at more negative voltages and turn off more slowly, and the current amplitude is increased. Although $HVCN1_L$ responds distinctly, the response of $HVCN1_S$ was consistently more profound. Because there is a tendency early in each experiment for proton currents to become larger and activate at more negative voltages as the amphotericin in the pipette solution improves electrical access to the cell membrane, and as pH_i is clamped to 7.0 by the applied NH_4^+ gradient (9, 10), the PMA response may be exaggerated if measurements are made before complete equilibration. A crucial quantitative control is to reverse the effects of PMA using the PKC inhibitor GF 109203X (GFX). The reversal of enhanced gating by GFX in both representative cells in Fig. 2 was complete, validating the responses.

SI Appendix, Fig. S3, shows normalized g_H-V relationships after the PMA response and after GFX treatment in all cells studied expressing $HVCN1_L$ or $HVCN1_S$. This comparison is more informative than control vs. PMA for reasons just discussed and because some cells were spontaneously active, as judged by GFX reversal being greater than the initial response to PMA. A possible spurious explanation for the greater PMA responsiveness of $HVCN1_S$ is that $HVCN1_L$ might have a greater tendency to activate spontaneously. *SI Appendix*, Fig. S3, does not support this view, verifying that $HVCN1_S$ is indeed more responsive.

SI Appendix, Fig. S4, summarizes the magnitude of the changes in four kinetic parameters of HVCN1 gating resulting from PMA and GFX treatment of cells expressing the two isoforms. For each parameter, the PMA response was significantly greater in $HVCN1_S$ than in $HVCN1_L$. Also for each parameter, GFX reversed the PMA response completely. In summary, $HVCN1_S$ channels exhibit a more profound response to phosphorylation than do $HVCN1_L$ channels.

Because B cells from CLL patients have higher-than-normal levels of $HVCN1_S$, their responsiveness might be enhanced. B cells from CLL patients and normal controls were studied by perforated-patch voltage clamp ($n = 4$ and 3, respectively), confirming that both CLL and normal B cells had proton currents that responded to PMA and GFX. Interestingly, CLL cells, which have a variable mixture of $HVCN1_S$ and $HVCN1_L$ (*SI Appendix*, Table S3), exhibited enhanced gating responses comparable with those of LK35.2 cells expressing $HVCN1_S$ exclusively (*SI Appendix*, Fig. S5), indicating that $HVCN1_S$ prevails in the response.

Identification of $HVCN1_S$ Phosphorylation Site. Two predicted high-probability PKC-δ phosphorylation sites exist in the N terminus of $HVCN1_L$ (11), Thr^{29} and Ser^{97}. We reported previously that both sites were phosphorylated after PMA exposure, but only Thr^{29} contributed detectably to the enhanced gating response of $HVCN1_L$ channels (11). Because the lack of the first 20 amino acids of the N terminus might result in different protein folding or architecture, it was important to examine the contribution of both corresponding sites in $HVCN1_S$, namely Thr^9 and Ser^{77}. We generated mutants that lacked one (T9A and S77A) or both (T9A/S77A) putative phosphorylation sites.

Cells with the T9A mutation ($n = 9$) and the double mutant T9A/S77A ($n = 5$) did not respond detectably to either PMA or GFX (*SI Appendix*, Fig. S6), implicating Thr^9 as crucial to the responses. In contrast, cells expressing the S77A mutant did respond to PMA and to GFX. Mean changes in parameter values are given in *SI Appendix*, Table S2. Therefore, the key residue in the PMA response is Thr^9 ($HVCN1_S$), the equivalent of Thr^{29} in $HVCN1_L$ channels (11). Any participation of Ser^{77} ($HVCN1_S$) or Ser^{97} ($HVCN1_L$) in the enhanced gating response was below our ability to detect it.

Intriguingly, T9A cells studied before stimulation exhibited ninefold faster activation and a 24-mV more negative $V_{threshold}$ than did unstimulated $HVCN1_S$ cells (*SI Appendix*, Table S1), resembling enhanced gating mode behavior. We reanalyzed data from analogous mutations studied previously in the full-length channel (11) and found that T29A also exhibited "enhanced gating" in unstimulated cells (*SI Appendix*, Table S1). Unstimulated "phosphomimetic" T29D cells exhibited weaker enhanced gating than T29A. Evidently, this Thr position is a potent determinant of gating kinetics. Together, these results suggest that phosphorylation of Thr^{29} in $HVCN1_L$ or Thr^9 in $HVCN1_S$ produces enhanced gating by a mechanism not simply involving the negative charge provided by the phosphate group. However, we cannot rule out

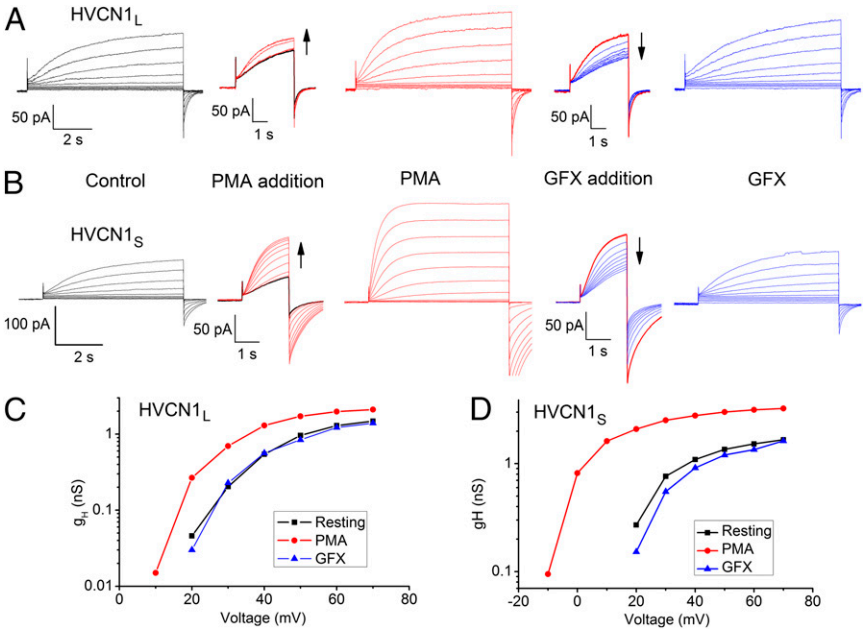

Fig. 2. $HVCN1_S$ responds more strongly to PMA stimulation than $HVCN1_L$. Perforated-patch voltage clamp was used to evaluate the electrophysiological properties of the two HVCN1 isoforms. Families of currents in 10-mV increments up to 70 mV from $V_{hold} = -40$ mV are shown in representative LK35.2 cells expressing $HVCN1_L$ (*A*) or $HVCN1_S$ (*B*) before stimulation, after application of the PKC activator PMA, and after inhibition of PKC by GF 109203X (GFX). Between the families are superimposed currents obtained during test pulses to 60 mV (for $HVCN1_L$) or 40 mV (for $HVCN1_S$) applied at 30-s intervals before and after addition of PMA or GFX to the bath solution. (*C* and *D*) Proton conductance–voltage relationships, g_H–V. The current amplitude was determined by extrapolating a single exponential fitted to the rising current, and g_H was calculated from the current using V_{rev} measured in each solution. Measurements were made in symmetrical pH 7.0 solutions containing 50 mM NH_4^+ to clamp pH_i (9).

the possibility that these mutations alter gating through a mechanism unrelated to that elicited by phosphorylation.

Because $HVCN1_S$ responded more strongly to PKC phosphorylation and the effect was mediated by phosphorylation of Thr^9 exclusively, we speculated that it could reflect increased phosphorylation of this residue. Indeed, our in vitro kinase assay showed that overall phosphorylation of wild-type $HVCN1_S$ was significantly higher than for wild-type $HVCN1_L$ (Fig. 3, *Left*, WT lanes). To assess phosphorylation of the critical PKC site mediating the enhanced-gating response, we carried out the same experiment with T29A (T9A for $HVCN1_S$), S97A (S77A for $HVCN1_S$), and T29A/S97A (T9A/S77A for $HVCN1_S$) mutants. As shown in Fig. 3, phosphorylation of the T9A mutant was reduced as much as for the T29A one, confirming that this Thr is phosphorylated by PKC in both isoforms. The analysis of the other PKC site mutant, S97A (S77A for $HVCN1_S$), and double mutants indicated a further reduction in overall phosphorylation, as we reported previously for $HVCN1_L$ (11), suggesting that Ser is also phosphorylated by PKC. However, as before, the patch-clamp experiments (*SI Appendix*, Fig. S6 and Table S1) indicated that phosphorylation of Thr^9 alone is responsible for the enhancement of $HVCN1_S$ proton currents.

$HVCN1_S$ Has a Weaker Association with the BCR than Does $HVCN1_L$. We found previously that HVCN1 was associated with the BCR in both normal and malignant B cells (3). The association causes HVCN1 to be internalized together with the BCR after its stimulation, an event that downregulates HVCN1 expression at the cell surface (3). Because the intracellular domains are likely to be the regions mediating the association with the BCR, we investigated if $HVCN1_S$ behaved differently from $HVCN1_L$. We overexpressed both isoforms in the B lymphoma cell line A20 D1.3 and assessed their expression at steady state and after BCR stimulation with a $F(ab')_2$ anti-IgM. Cells expressed similar levels of HVCN1, IgM, and the BCR coreceptor CD79B (*SI Appendix*, Fig. S7 *A–C*). We did not note significant differences in the pattern of expression of the two isoforms at steady state. Importantly, however, upon BCR stimulation, the extent of HVCN1 internalization for the two isoforms appeared different (Fig. 4*A*). Quantification of the immunofluorescence staining showed a significantly larger percentage of internalized HVCN1 in cells expressing $HVCN1_L$ compared with $HVCN1_S$ (36 vs. 25%, Fig. 4*A*, *Upper* graph). Furthermore, the extent of colocalization with IgM was also reduced from 0.562 to 0.407 (Fig. 4*A*, *Lower* graph). Diminished $HVCN1_S$ internalization was not due to reduced IgM internalization, which was actually increased, compared with cells overexpressing $HVCN1_L$ (*SI Appendix*, Fig. S7*D*). These data indicate that $HVCN1_S$ association with the BCR is different and that this results in increased localization of proton channels at the plasma membrane.

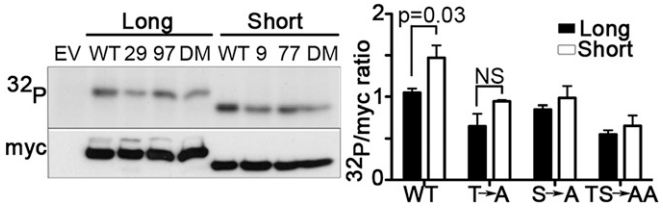

Fig. 3. $HVCN1_S$ is phosphorylated more by PKC-δ than $HVCN1_L$. PKC-δ in vitro kinase assay showing phosphorylation of $HVCN1_L$ and $HVCN1_S$ wild type ("WT"), single mutants T29A ("29") or T9A for $HVCN1_S$ ("9"), S97A ("97") or S77A for $HVCN1_S$ ("77"), and double mutants T29A/S97A and T9A/S77A for $HVCN1_S$ ("DM"). The assay was carried out with recombinant $HVCN1_L$ and $HVCN1_S$ expressed in HEK293T cells and immunoprecipitated with an anti-myc antibody. Cells transfected with an empty vector ("EV") were used as negative control. The myc immunoblot indicates loading. Bars represent the densitometry analysis of the ^{32}P-HVCN1 versus myc-HVCN1 of three independent experiments (mean ± SEM). NS, not significant.

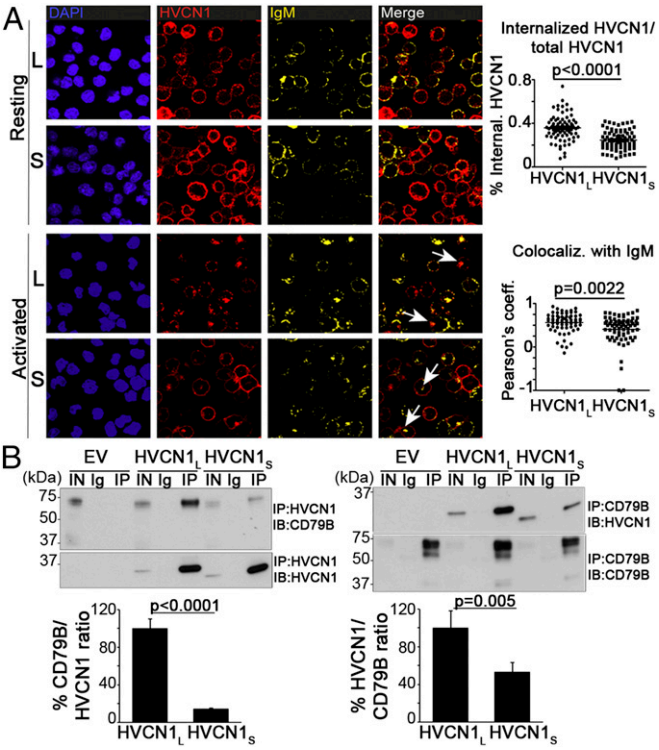

Fig. 4. $HVCN1_S$ is associated and internalized with the BCR to a lesser extent compared with $HVCN1_L$. (*A*, *Left*) Confocal images of A20 D1.3 cells overexpressing $HVCN1_L$ or $HVCN1_S$ at steady state ("resting" panels) or 30 min after activation with an anti-IgM crosslinking $F(ab')_2$ fragment ("activated" panels). Merge panels represent IgM and HVCN1 staining. White arrows indicate cointernalized HVCN1 and IgM. (Right) Quantification of percentage of internalized HVCN1 (*Upper* graph) and colocalization coefficient for HVCN1 and IgM (*Lower* graph). Each symbol represents a single cell [n = 78 (*Upper*); n = 67 (*Lower*)], and horizontal lines indicate the mean. Pearson's colocalization coefficient (0, no colocalization; 1, total colocalization). (*B*) Coimmunoprecipitation of overexpressed $HVCN1_L$ or $HVCN1_S$ and endogenous CD79B (Ig-associated-β or Ig-β). Proteins were coimmunoprecipitated from A20 D1.3 cells and analyzed by immunoblot in nonreducing conditions. EV, cells transduced with empty vector; IN, input cell lysate (2% of the cell lysate used for immunoprecipitation); Ig, negative control beads conjugated to mouse or rat IgG; IP, immunoprecipitation; IB, immunoblot. Graphs represent densitometry analysis of both co-IP experiments (mean ± SEM, three independent experiments).

To determine the reason for the different association of HVCN1 isoforms with the BCR, we carried out a coimmunoprecipitation (co-IP) with an anti-CD79B and the reciprocal experiment with an anti-myc (for the myc-tagged HVCN1 isoforms). As shown in Fig. 4*B*, interaction of $HVCN1_S$ with CD79B was indeed significantly weaker with both co-IP assays. The differences between the two antibodies are likely due to differences in the efficiency of pull down (with the anti-myc being more efficient than the anti-CD79B). Overall, these data show that the first 20 amino acids present in $HVCN1_L$ are critical for the association with the BCR and that their absence in $HVCN1_S$ results in greater expression of this isoform at the plasma membrane after BCR stimulation.

$HVCN1_S$ Expression Is Enriched in CLL Cells. Given the increased expression of $HVCN1_S$ in B-cell lines and in CLL samples (Fig. 1*A*), combined with its ability to mediate stronger proton currents (Fig. 2), we investigated whether its expression could have an impact on CLL disease progression. To this end, we analyzed the expression of $HVCN1_S$ in a cohort of 76 samples of peripheral

PHYSIOLOGY

blood CLL cells with annotated clinical data. Details of the patients' characteristics are reported in *SI Appendix*, Table S3. The samples investigated showed variable expression of both isoforms, with an average ratio of $HVCN1_S$ to $HVCN1_L$ of 0.52 ± 0.034 (mean ± SE). As shown in Fig. 1*A*, $HVCN1_S$ was markedly higher in CLL than in primary B cells from healthy donors, in which $HVCN1_S$ is barely detectable. Given the wide range of $HVCN1_S$ expression in CLL cells, we split samples in two groups, one with a ratio of $HVCN1_S/HVCN1_L$ below the median value of 0.477 (i.e., with lower expression of $HVCN1_S$) and one with higher $HVCN1_S$ expression (above the median). A Kaplan–Meier curve for overall survival showed that patients with higher expression of $HVCN1_S$ had reduced overall survival, although differences did not reach statistical significance (*SI Appendix*, Fig. S8). We further analyzed the data specifically for the two main subgroups of CLL patients: those presenting a mutated variable region in the BCR heavy chain (*IGHV*) and those with an unmutated *IGHV*. Given the small number of samples for which we knew the mutation status (*SI Appendix*, Fig. S8 and Table S3), it was not surprising that differences did not reach statistical significance; nonetheless, higher expression of $HVCN1_S$ tended to correlate with a poorer outcome in both groups.

$HVCN1_S$ Expression Results in Stronger BCR-Dependent Signaling, Proliferation, and Chemokine-Dependent Migration. To establish if $HVCN1_S$ could confer a growth advantage to malignant B cells, we first assessed BCR-dependent signaling in A20 D1.3 cells transduced with empty vector (EV), $HVCN1_L$, and $HVCN1_S$. As shown in Fig. 5*A*, the presence of $HVCN1_S$ resulted in more prolonged activation of the extracellular signal-regulated kinase (Erk), which is responsible for the upregulation of several anti-apoptotic proteins in CLL cells (12). Furthermore, to determine if the two proton channel isoforms regulated cell proliferation, we measured the extent of EdU incorporation, a nucleoside analog included in nascent DNA. Interestingly, only $HVCN1_S$ provided a significant advantage compared with EV cells (Fig. 5*B*).

Another important property of CLL cells is the ability to respond to the chemokine CXCL12 [chemokine (C-X-C motif) ligand 12], which affects their migration, homing, and survival (13). Because HVCN1 was shown to regulate migration of breast (5) and colorectal cancer cells (6), we set out to characterize if HVCN1 isoforms affected chemokine-dependent migration in a B-cell setting. As Fig. 5*C* shows, both $HVCN1_L$ and $HVCN1_S$ expression resulted in increased migration to CXCL12; however, only $HVCN1_S$ resulted in a significant advantage. Taken together, these data indicate that $HVCN1_S$ promotes malignant B-cell survival through enhanced proliferation and migration.

Discussion

Only one proton channel gene has been identified in any species. However, the human gene can generate two different isoforms, $HVCN1_L$ and $HVCN1_S$ (3). In this paper, we confirmed the existence of alternative splicing variants as reported in the GenBank database, presenting evidence that translation of $HVCN1_S$ starts at an alternative ATG. The resulting protein is 20 amino acids shorter at the N terminus, as confirmed here by immunoblotting with an antibody raised against the first 20 amino acids of full-length HVCN1 ($HVCN1_L$). Compared with peripheral B cells from healthy donors, B-cell lines and CLL cells showed increased expression of total HVCN1 due to an upregulation of $HVCN1_S$. Higher levels of $HVCN1_S$ tended to correlate with decreased overall survival in a cohort of 76 blood samples from CLL patients. Given the wide range of expression of $HVCN1_S$ in CLL and the limited number of samples analyzed, it would be necessary to screen a much larger panel of samples to determine if this trend is significant. This would be particularly interesting for the mutated CLL subgroup because these patients have a more favorable prognosis overall; however, some still present more aggressive disease, and markers to identify this subpopulation are lacking.

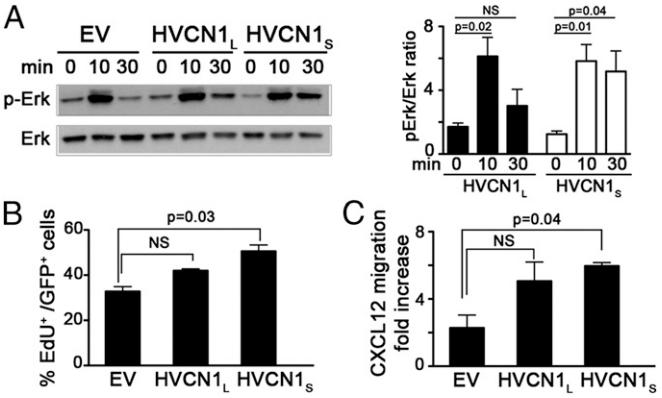

Fig. 5. $HVCN1_S$ expression modulates BCR signaling, cell proliferation, and migration. (*A*) BCR stimulation with 20 μg/mL $F(ab')_2$ anti-IgM in A20 D1.3 cells overexpressing empty vector (EV), $HVCN1_L$, and $HVCN1_S$. Immunoblot showing phosphorylated Erk (p-Erk) and total Erk. Bars indicate the ratio of the densitometry analysis of p-Erk versus total Erk from three independent experiments (mean ± SEM). (*B*) Proliferation of A20 D1.3 cells assessed by EdU incorporation after 3 h of incubation. Results are shown as percentage of Edu^+ cells versus total number of GFP^+ cells of two independent experiments (mean ± SEM). (*C*) Transwell chamber assay of migration toward the chemokine CXCL12. Migrated cells were counted after 4 h. Results are shown as fold increase of migrated cells in the presence of CXCL12 versus media alone. Data represent the average of two experiments (mean ± SEM).

Comparison of their electrophysiological properties revealed that $HVCN1_S$ channels open about twice as slowly as $HVCN1_L$ channels. A more profound difference was seen in response to stimulation by PMA. Agonists that activate PKC strongly amplify the proton conductance in many human and mammalian cells (8, 9, 14–18), a phenomenon called "enhanced gating." Although both isoforms responded to PMA, the $HVCN1_S$ response was significantly greater. This differential responsiveness enables cells to modulate proton channel activity by preferential expression of $HVCN1_S$ or $HVCN1_L$ isoforms. That the PMA response of CLL cells resembled that of LK35.2 cells expressing exclusively $HVCN1_S$ reveals that, in a mixture of isoforms, $HVCN1_S$ will dominate due to its lower $V_{threshold}$.

The distinct gating of the two isoforms $HVCN1_S$ and $HVCN1_L$ that differ only in the first 20 amino acids of the N terminus emphasizes the importance of this intracellular domain in modulating gating kinetics. Proton channels are thought to open as a result of outward movement of the S4 transmembrane helix (19–21). Being an extension of the S4 helix, the C terminus affects gating directly (22). Nevertheless, gating kinetics is modulated drastically (*i*) in the enhanced gating mode by phosphorylation of Thr^{29} (11), (*ii*) by the point mutation T9A in $HVCN1_S$ or T29A in $HVCN1_L$ (*SI Appendix*, Table S1), and (*iii*) in the naturally occurring mutation M91T (23), all of which are localized to the N terminus.

Because T9A and T9A/S77A mutants failed to respond to PMA or GFX, enhanced gating of $HVCN1_S$ is evidently mediated entirely by phosphorylation of Thr^9. This residue is equivalent to Thr^{29}, the key phosphorylation site producing enhanced gating in $HVCN1_L$ (11). Here we show that phosphorylation of Thr^9 and overall phosphorylation is greater in $HVCN1_S$ than in $HVCN1_L$, suggesting that the loss of the first 20 amino acids facilitates phosphorylation of this residue. Additionally, the mechanism by which phosphothreonine orchestrates enhanced gating may be modified in $HVCN1_S$. Whether the two isoforms are phosphorylated at steady state in tumor B cells will depend upon expression and activation of PKC in these cells. Because PKC was expressed and activated in the great majority of CLL

samples investigated (*SI Appendix*, Table S3), we believe constitutive phosphorylation of proton channels in CLL cells to be highly likely.

Furthermore, we present evidence that $HVCN1_S$ has a weaker association with the BCR, which results in greater expression at the plasma membrane and reduced internalization upon BCR stimulation. Evidently, the first 20 amino acids of HVCN1 are important for association with the BCR. It will be interesting to investigate which residues in HVCN1 are involved in this interaction and whether there is a direct association with the BCR complex (either the Ig or the coreceptors CD79A and CD79B) or if additional scaffolding proteins are involved. Malignant B cells such as CLL cells are stimulated through their BCR in the tumor microenvironment, and each round of stimulation normally results in BCR internalization (4). That tumor B cells upregulate an isoform of HVCN1 that remains preferentially at the plasma membrane after BCR stimulation suggests that these cells might find plasma membrane expression of $HVCN1_S$ beneficial to their growth. This is corroborated by the advantage in BCR-dependent Erk activation, proliferation, and chemokine-dependent migration conferred by $HVCN1_S$. Higher levels of HVCN1 expression correlate with metastatic tendency and poor prognosis in breast cancer (5) and colorectal cancer (6) although the isoform involved has not been reported.

Overall, our data show the existence of a shorter isoform of HVCN1 with enhanced gating responses that is specifically enriched in malignant B cells. The enhanced gating of $HVCN1_S$ produces larger proton currents in CLL cells that may contribute to the pathology, as suggested by stronger BCR signaling, increased cell proliferation, and chemokine response provided by $HVCN1_S$ expression.

Materials and Methods

Cell Lines and Plasmids. The mouse B lymphoma cell lines LK35.2 HyHEL10 (IgG2a, κ-chain; H-2^{kxd}) and A20 D1.3 (IgG2a, κ-chain; H-2^{d}) overexpressing recombinant IgM receptors were a gift from F. Batista (London Research Institute, London). The cells were transduced with MigRI retroviral vectors coding for myc-tagged $HVCN1_L$ or $HVCN1_S$. T29A (T9A for $HVCN1_S$), S97A (S77A for $HVCN1_S$), and T29A/S97A (T9A/S77A for $HVCN1_S$) mutants were generated using a QuikChange site-directed mutagenesis kit (Stratagene). The retroviral particles were produced in the Phoenix α packaging cell line as described elsewhere (11).

Phosphorylation Assay. HEK293T cells were transfected by Ca^{2+} phosphate with myc-tagged $HVCN1_L$, $HVCN1_S$, and mutant plasmids. Forty-eight hours after transfection, cells were lysed in 20 mM Hepes, 1% Triton X-100, 137 mM NaCl, 2.5 mM β-glycerophosphate, 1 mM Na_3VO_4, 2 mM EDTA, and proteases inhibitors (Sigma Aldrich). One milligram of proteins was immunoprecipitated with anti-myc tag antibody (9B11, Cell Signaling Technology) conjugated to protein-G Sepharose beads for 1 h. After washing with lysis buffer, beads were incubated in 40 μL kinase assay buffer [20 mM Hepes, 1 mM EGTA, 0.4 mM EDTA, 5 mM $MgCl_2$, 0.1 mM $CaCl_2$, 0.05 mM DTT, 0.1 mg/mL phosphatidylserine, 0.01 mg/mL diacylglycerol, 2.5 mM β-glycerophosphate, 1 μM PMA, 100 nM PKC-δ (Millipore), 100 μM cold ATP, and 10 μCi of [γ-^{32}P]ATP (Perkin-Elmer)] for 20 min at 30 °C. The reaction was stopped by resuspending beads in 2× Laemmli sample buffer. Samples were then separated by SDS/PAGE, transferred to a nitrocellulose membrane, and exposed to X-ray films. Membranes were immunoblotted with anti-myc antibody to determine loading.

Electrophysiology. Whole-cell or perforated-patch variants of the patch-clamp technique were carried out as described in detail previously (24). Perforated-patch studies included ~225 μM amphotericin B in the pipette to permeabilize the patch membrane, and 50 mM NH_4^+ to clamp pH_i to pH_o. For whole-cell studies, the main pipette solution (also used externally) contained (in mM) 130 $TMACH_3SO_3$, 2 $MgCl_2$, 2 EGTA, and 80 MES, titrated to pH 5.5 with ~20 tetramethylammonium hydroxide (TMAOH). Bath solutions at pH 7.0 had (in mM) 90 $TMACH_3SO_3$, 3 $CaCl_2$, 1 EGTA, 100 *N*,*N*-Bis-(2-hydroxyethyl)-2-aminoethanesulfonic acid (BES), and 36–40 TMAOH. When pH was varied, the following buffers with pK_a near the desired pH were used: Homopipes for pH 4.6, MES for pH 5.5–6.0, BisTris for pH 6.5, Hepes for pH 7.5, and Tricine for pH 8.0. Experiments were done at 21 °C or at room temperature (20–25 °C). No leak correction has been applied to current records.

Patch-Clamp Studies of CLL and Healthy B Cells. Cells were shipped frozen on dry ice. After thawing, cells were suspended in RPMI with serum, centrifuged at 1,100 × *g* for 5 min, and resuspended in a small volume (1–2 mL) of RPMI with serum.

Statistics. Statistical analysis was carried out by Student's unpaired *t* test. Further materials and methods are provided in *SI Appendix*.

ACKNOWLEDGMENTS. M.C. is the recipient of a Bennett Fellowship from Leukaemia and Lymphoma Research (ref. 12002). M.A.B. is supported by a GlaxoSmithKline Oncology–Biotechnology and Biological Sciences Research Council Collaborative Awards in Science and Engineering PhD studentship. This work was supported by National Institutes of Health Grants GM087507 and GM102336 (to T.E.D.).

1. Musset B, et al. (2011) Aspartate 112 is the selectivity filter of the human voltage-gated proton channel. *Nature* 480(7376):273–277.
2. DeCoursey TE (2013) Voltage-gated proton channels: Molecular biology, physiology, and pathophysiology of the H_V family. *Physiol Rev* 93(2):599–652.
3. Capasso M, et al. (2010) HVCN1 modulates BCR signal strength via regulation of BCR-dependent generation of reactive oxygen species. *Nat Immunol* 11(3):265–272.
4. Stevenson FK, Krysov S, Davies AJ, Steele AJ, Packham G (2011) B-cell receptor signaling in chronic lymphocytic leukemia. *Blood* 118(16):4313–4320.
5. Wang Y, Li SJ, Wu X, Che Y, Li Q (2012) Clinicopathological and biological significance of human voltage-gated proton channel Hv1 protein overexpression in breast cancer. *J Biol Chem* 287(17):13877–13888.
6. Wang Y, Wu X, Li Q, Zhang S, Li SJ (2013) Human voltage-gated proton channel Hv1: A new potential biomarker for diagnosis and prognosis of colorectal cancer. *PLoS ONE* 8(8):e70550.
7. Cherny VV, Markin VS, DeCoursey TE (1995) The voltage-activated hydrogen ion conductance in rat alveolar epithelial cells is determined by the pH gradient. *J Gen Physiol* 105(6):861–896.
8. Morgan D, et al. (2007) Sustained activation of proton channels and NADPH oxidase in human eosinophils and murine granulocytes requires PKC but not $cPLA_2$ α activity. *J Physiol* 579(Pt 2):327–344.
9. DeCoursey TE, Cherny VV, Zhou W, Thomas LL (2000) Simultaneous activation of NADPH oxidase-related proton and electron currents in human neutrophils. *Proc Natl Acad Sci USA* 97(12):6885–6889.
10. Grinstein S, Romanek R, Rotstein OD (1994) Method for manipulation of cytosolic pH in cells clamped in the whole cell or perforated-patch configurations. *Am J Physiol* 267(4 Pt 1):C1152–C1159.
11. Musset B, et al. (2010) Identification of Thr^{29} as a critical phosphorylation site that activates the human proton channel *Hvcn1* in leukocytes. *J Biol Chem* 285(8):5117–5121.
12. Efremov DG, Gobessi S, Longo PG (2007) Signaling pathways activated by antigen-receptor engagement in chronic lymphocytic leukemia B-cells. *Autoimmun Rev* 7(2):102–108.
13. Burger JA, Kipps TJ (2002) Chemokine receptors and stromal cells in the homing and homeostasis of chronic lymphocytic leukemia B cells. *Leuk Lymphoma* 43(3):461–466.
14. Bánfi B, et al. (1999) A novel H^+ conductance in eosinophils: Unique characteristics and absence in chronic granulomatous disease. *J Exp Med* 190(2):183–194.
15. DeCoursey TE, Cherny VV, DeCoursey AG, Xu W, Thomas LL (2001) Interactions between NADPH oxidase-related proton and electron currents in human eosinophils. *J Physiol* 535(Pt 3):767–781.
16. Mori H, et al. (2003) Regulatory mechanisms and physiological relevance of a voltage-gated H^+ channel in murine osteoclasts: Phorbol myristate acetate induces cell acidosis and the channel activation. *J Bone Miner Res* 18(11):2069–2076.
17. Musset B, Cherny VV, DeCoursey TE (2012) Strong glucose dependence of electron current in human monocytes. *Am J Physiol Cell Physiol* 302(1):C286–C295.
18. Musset B, et al. (2008) A pH-stabilizing role of voltage-gated proton channels in IgE-mediated activation of human basophils. *Proc Natl Acad Sci USA* 105(31):11020–11025.
19. Gonzalez C, Rebolledo S, Perez ME, Larsson HP (2013) Molecular mechanism of voltage sensing in voltage-gated proton channels. *J Gen Physiol* 141(3):275–285.
20. Kulleperuma K, et al. (2013) Construction and validation of a homology model of the human voltage-gated proton channel hH_V1. *J Gen Physiol* 141(4):445–465.
21. Takeshita K, et al. (2014) X-ray crystal structure of voltage-gated proton channel. *Nat Struct Mol Biol* 21(4):352–357.
22. Fujiwara Y, Kurokawa T, Okamura Y (2014) Long α helices projecting from the membrane as the dimer interface in the voltage-gated H^+ channel. *J Gen Physiol* 143(3):377–386.
23. Iovannisci D, Illek B, Fischer H (2010) Function of the HVCN1 proton channel in airway epithelia and a naturally occurring mutation, M91T. *J Gen Physiol* 136(1):35–46.
24. Morgan D, Cherny VV, Murphy R, Katz BZ, DeCoursey TE (2005) The pH dependence of NADPH oxidase in human eosinophils. *J Physiol* 569(Pt 2):419–431.

PHYSIOLOGY

Supporting Information

Enhanced activation of an amino-terminally truncated isoform of voltage-gated proton channel HVCN1 enriched in malignant B cells

Elayne Hondares, Mark Brown, Boris Musset, Deri Morgan, Vladimir V. Cherny, Christina Taubert, Mandeep K. Bhamrah, David Coe, Federica Marelli-Berg, John G. Gribben, Martin J.S. Dyer, Thomas E. DeCoursey, Melania Capasso

SUPPORTING FIGURES

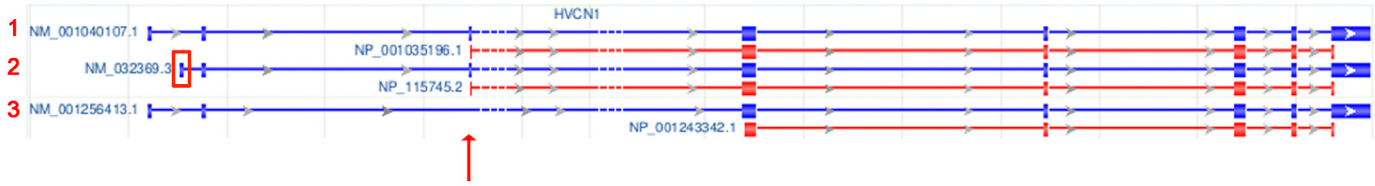

Fig. S1. Alignment of the 5′ regions of the three mRNA isoforms reported in the NCBI DNA and RNA database for human HVCN1. The blue lines represent mRNA and the red line protein (coding) sequences. The thicker regions indicate the exons, whereas the thinner regions correspond to the gene introns. We have included a red box to highlight the alternative 5′-UTR utilized by variant 2 and an arrow to indicate the missing exon in variant 3. Source: NCBI DNA and RNA database.

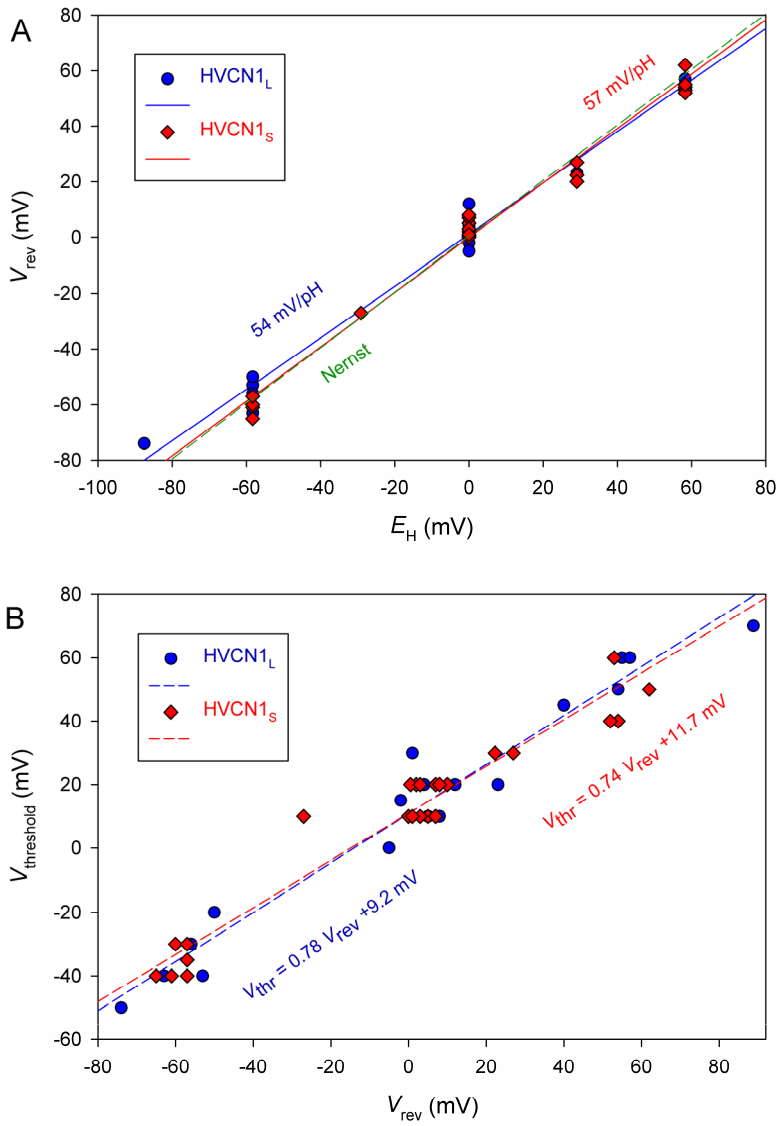

Fig. S2. A) Both HVCN1$_L$ (●) and HVCN1$_S$ (♦) are proton selective. In whole-cell configuration, V_{rev} was determined using tail currents. The range of pH_o studied was 4.6-8.0; the range of pH_i was 6.5-7.0. Lines show linear regression on each set, with slopes 52 mV (HVCN1$_L$) and 57.2 mV (HVCN1$_S$), compared with 58.2 mV calculated by the Nernst equation. B) The ΔpH dependence of gating of HVCN1$_L$ (●) and HVCN1S channels (♦) studied in whole-cell configuration is indistinguishable. The threshold voltage at which current is first activated, $V_{threshold}$, is plotted as a function of the measured V_{rev}. Dashed lines show linear regression on the data, with the equations provided. Identification of $V_{threshold}$ was based on the appearance of time dependent currents during test pulses, as well as the appearance of distinct tail currents upon repolarization.

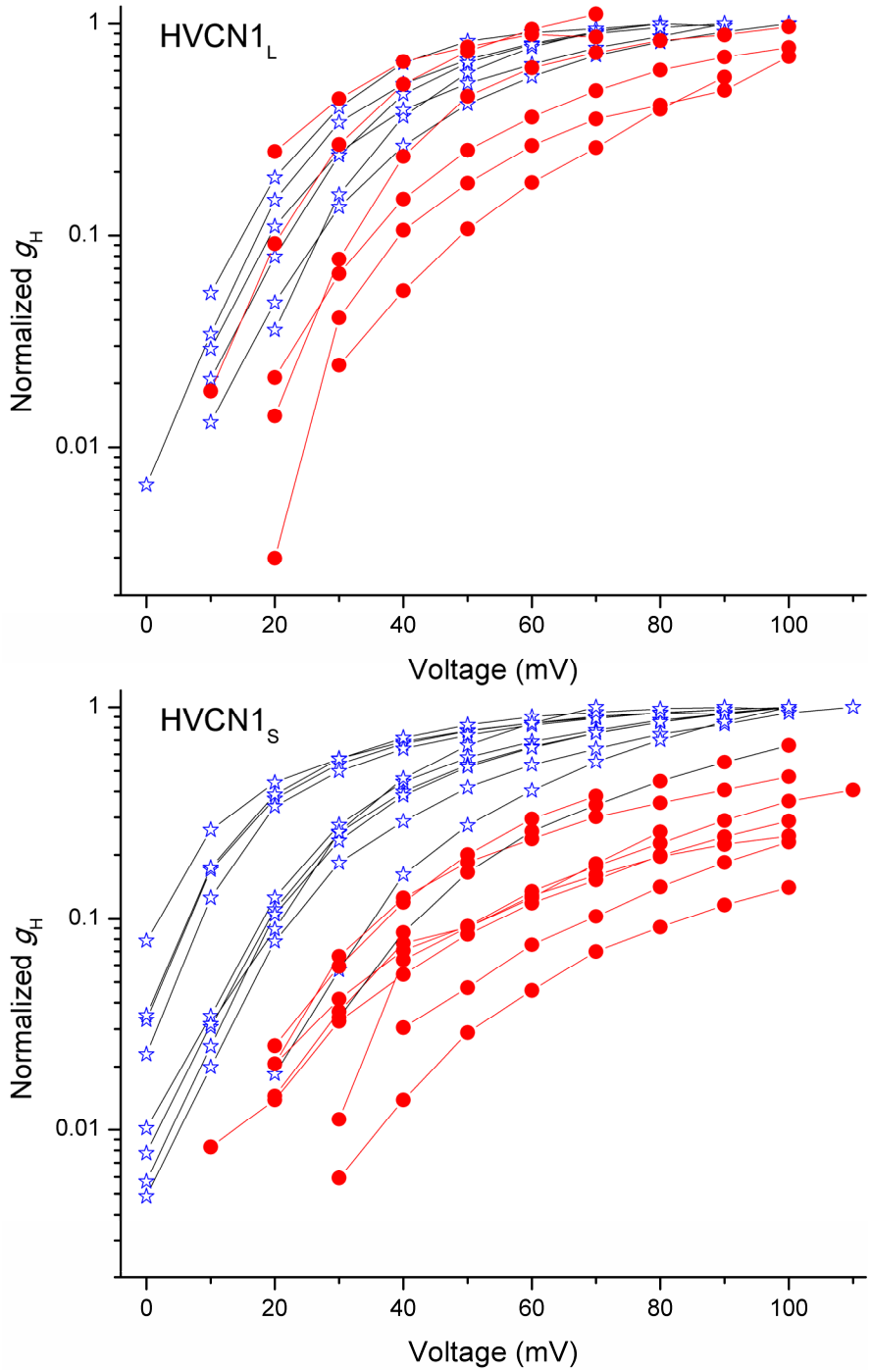

Fig. S3. HVCN1$_L$ responds to PMA stimulation, but HVCN1$_S$ responds more strongly. Plotted are g_H-V relationships in individual cells, connected by lines, normalized to the maximal value after PMA stimulation (blue stars). For each cell, the g_H-V relationship after GFX is also plotted (●). Although both isoforms respond, the increase in $g_{H,max}$ and the negative shift by PMA are both more profound in HVCN1$_S$.

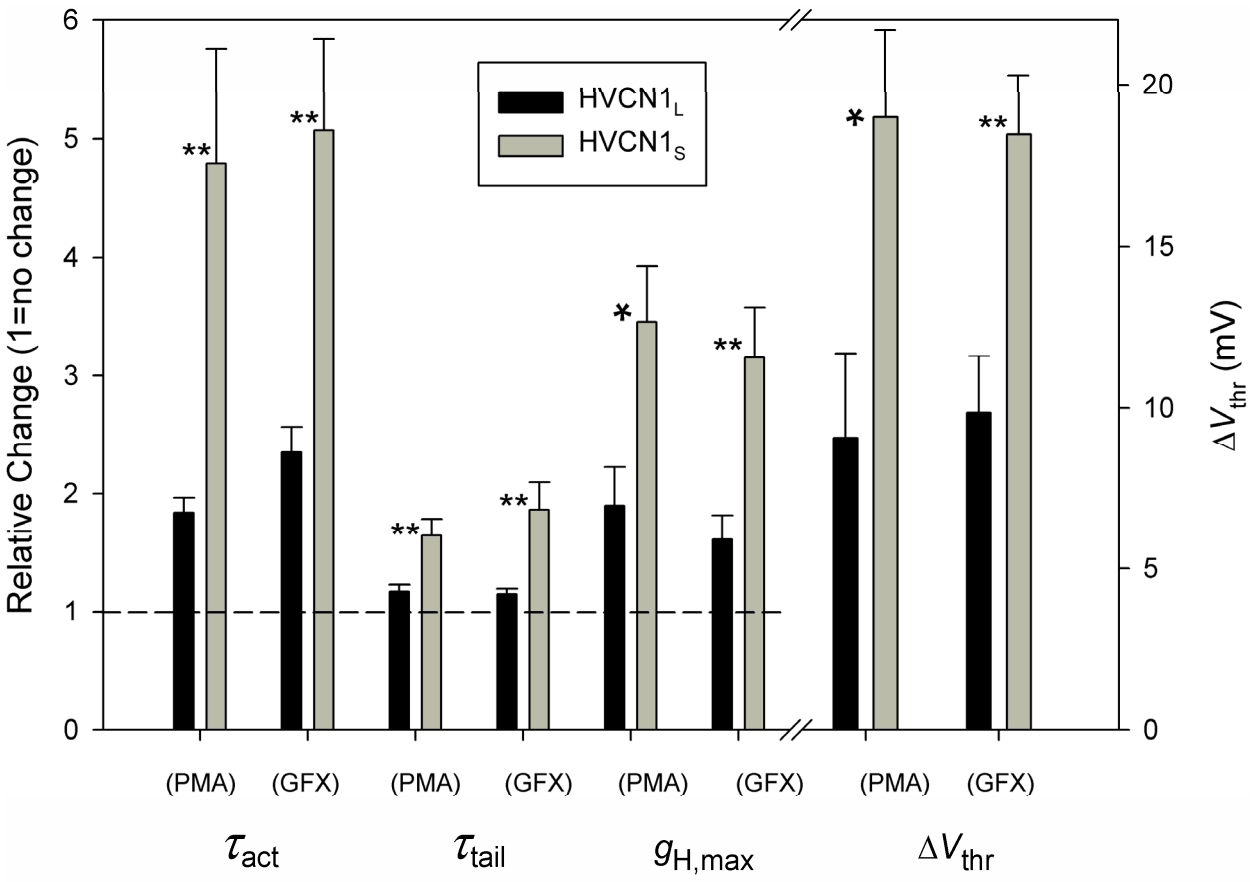

Fig. S4. The enhanced gating mode is more pronounced in $HVCN1_S$ (gray bars) than in $HVCN1_L$ (black). Mean ± SEM (n = 13-18 for $HVCN1_L$, 13-15 for $HVCN1_S$) changes produced in the four properties that differ in the enhanced gating mode are summarized. For each of the first three parameters, the relative change is plotted so that the effect increases relative to 1.0 (dashed reference line); the ratio for τ_{act} is (control/PMA), for τ_{tail} is (PMA/control), for $g_{H,max}$ is (control/PMA). Similarly, for GFX reversal, the ratio for τ_{act} is (GFX/PMA), for τ_{tail} is (PMA/GFX), for $g_{H,max}$ is (GFX/PMA). For the shift in $V_{threshold}$ the values show the absolute magnitude of the negative shift produced by PMA and the positive shift produced by GFX. For each parameter, the $HVCN1_S$ response is significantly greater than the $HVCN1_L$ response (*p<0.05, **p<0.01). For each parameter, the reversal by GFX is not significantly different from the effect of PMA.

In many human and mammalian cells, stimulation by agonists that act through activation of PKC results in strong amplification of the proton conductance (1-8), a phenomenon that has been called “enhanced gating.” Enhanced gating encompasses a predictable constellation of changes in the properties of proton channels (described in

this table); however, there are two subtypes of enhanced gating. In the full enhanced gating mode $V_{threshold}$ shifts by -30 to -40 mV, τ_{act} speeds typically 3-5-fold, τ_{tail} slows up to 3-5 fold, and $g_{H,max}$ increases by 2-4-fold. The full response occurs in cells with a high level of NADPH oxidase (NOX) activity; agents that activate NOX also produce enhanced gating of HVCN1 (9). Cells exhibiting a full response include human eosinophils (1, 2, 5, 10), neutrophils (3), monocytes (7), PLB-985 cells (11), and sperm (4), and mouse granulocytes (5), osteoclasts (6), and perhaps dendritic cells (12). A modified degree of enhanced gating occurs in cells lacking NOX activity; typically the g_H-V relationship shifts by -20 mV or less and τ_{tail} slows little or not at all (13). The PMA response observed here in cells expressing $HVCN1_S$ fits this pattern precisely, with a 5-fold speeding of τ_{act}, and a 3-fold increase in $g_{H,max}$, but τ_{tail} slowed less than 2-fold, and the g_H-V relationship shifted only -20 mV. Other cells that exhibit a partial response include human neutrophils from CGD patients lacking $gp91^{phox}$, PLB-985 cells with $gp91^{phox}$ knocked out (11), and human basophils (8). The PMA response observed here in $HVCN1_S$ is consistent with the low level of ROS production by LK35.2 cells.

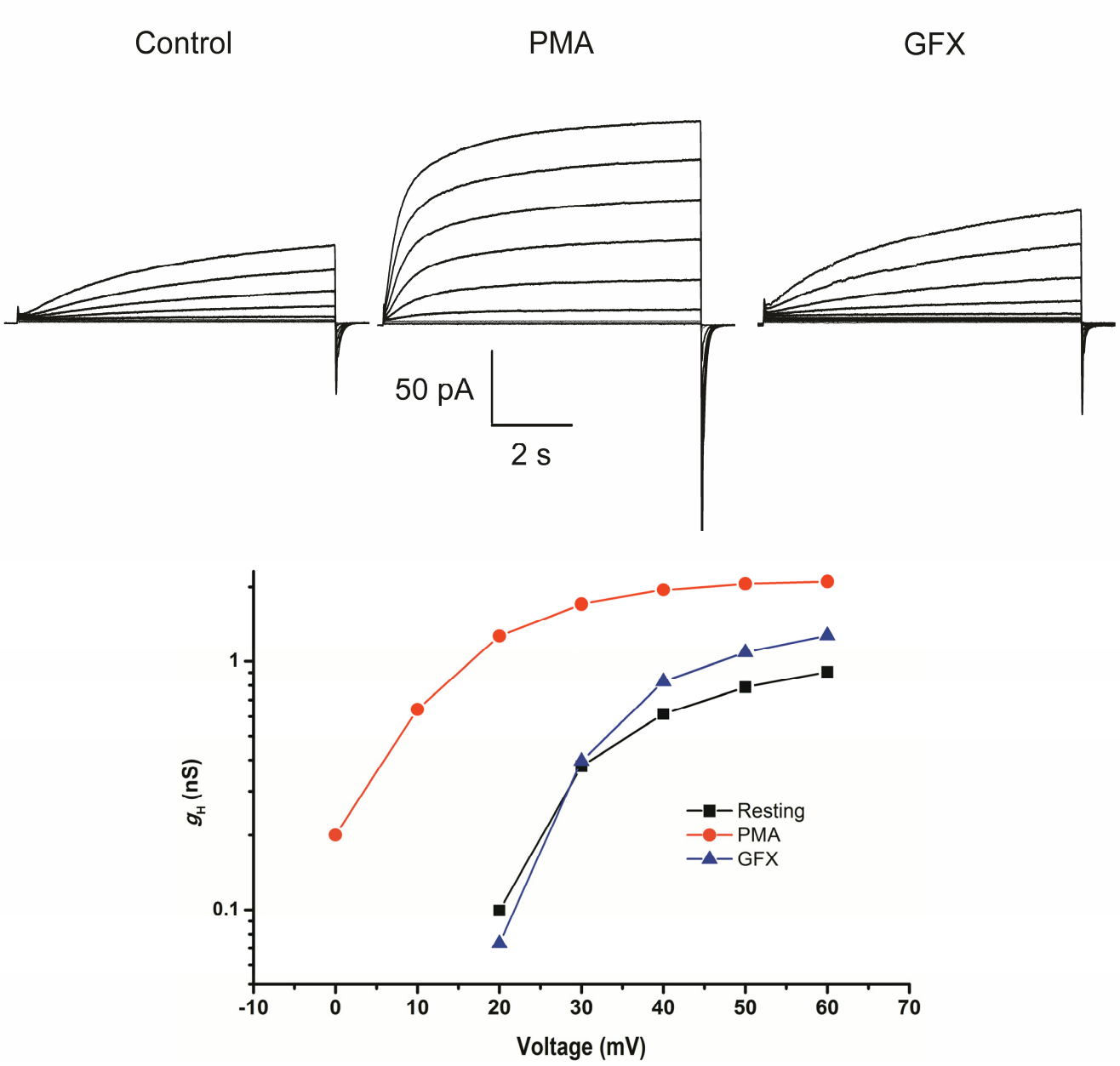

Fig. S5. Enhanced gating of proton channels in response to PMA and its reversal by GFX are illustrated in a B cell from a patient with CLL. Each family of currents was recorded during pulses from a holding potential of -40 mV in 10 mV increments up to 60 mV. The graph shows a large negative shift of the g_H-V relationship produced by PMA, and its complete reversal by GFX. Similar responses were observed in cells from three other patients. In 4 CLL cells (each from a different patient) τ_{act} was 4.0 ± 0.9 times faster and the mean $V_{threshold}$ shift was 18.8 ± 4.3 mV (mean ± SEM).

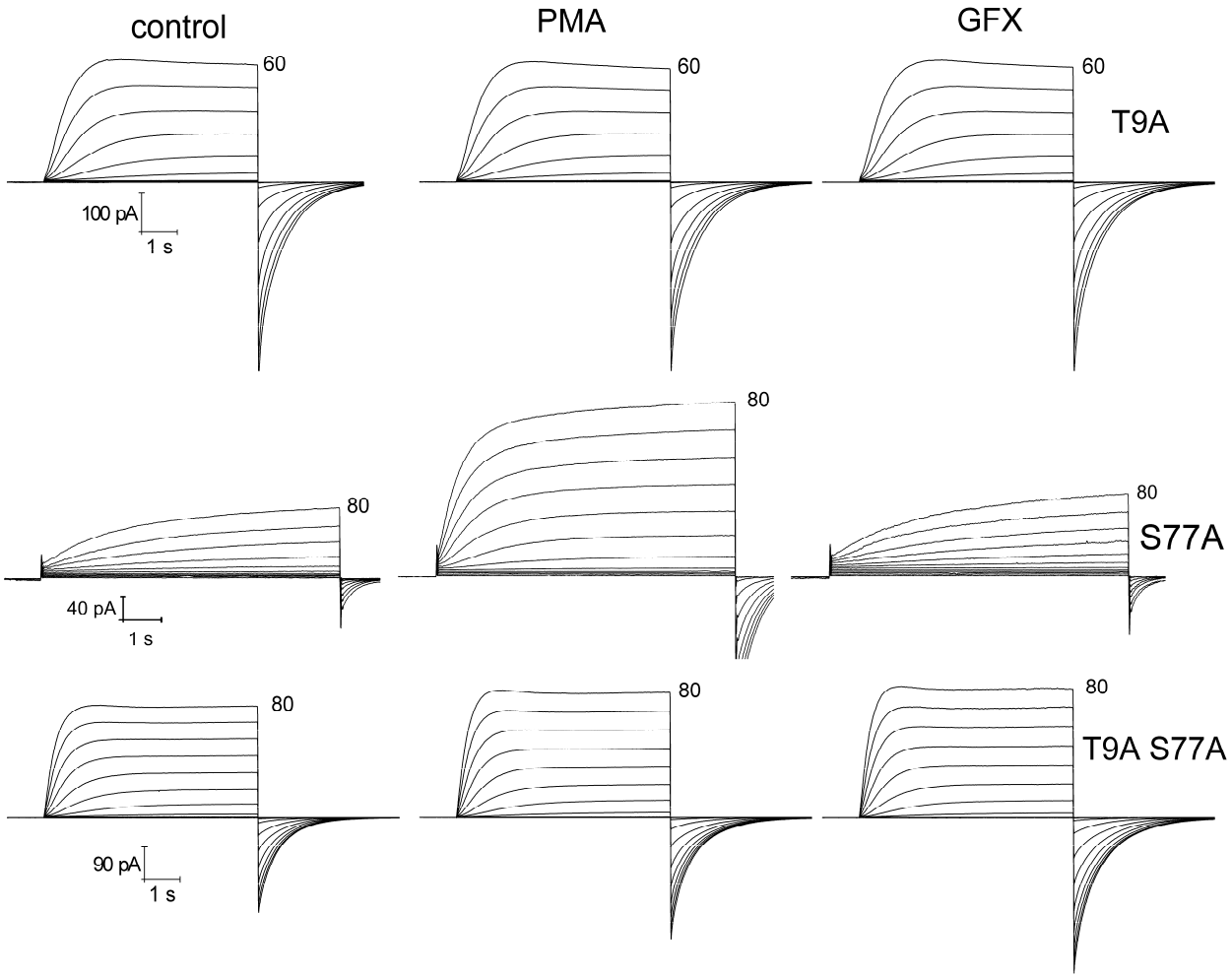

Fig. S6. The responses to PMA and GFX in three mutants of $HVCN1_S$. The T9A mutant of $HVCN1_S$ does not respond to PMA or GFX. The S77A mutant of $HVCN1_S$ responds distinctly to PMA and GFX, whereas the double mutant T9A/S77a also fails to respond. These results implicate Thr^9 as essential to the enhanced gating response. Families of currents in the same cell during identical voltage pulses before stimulation, after PMA, and after GFX treatment are shown for representative cells. Each cell was held at -40 mV and pulses were applied in 10 mV increments up to the indicated voltage. Note the rapid activation of cells with the T9A mutation (single or double).

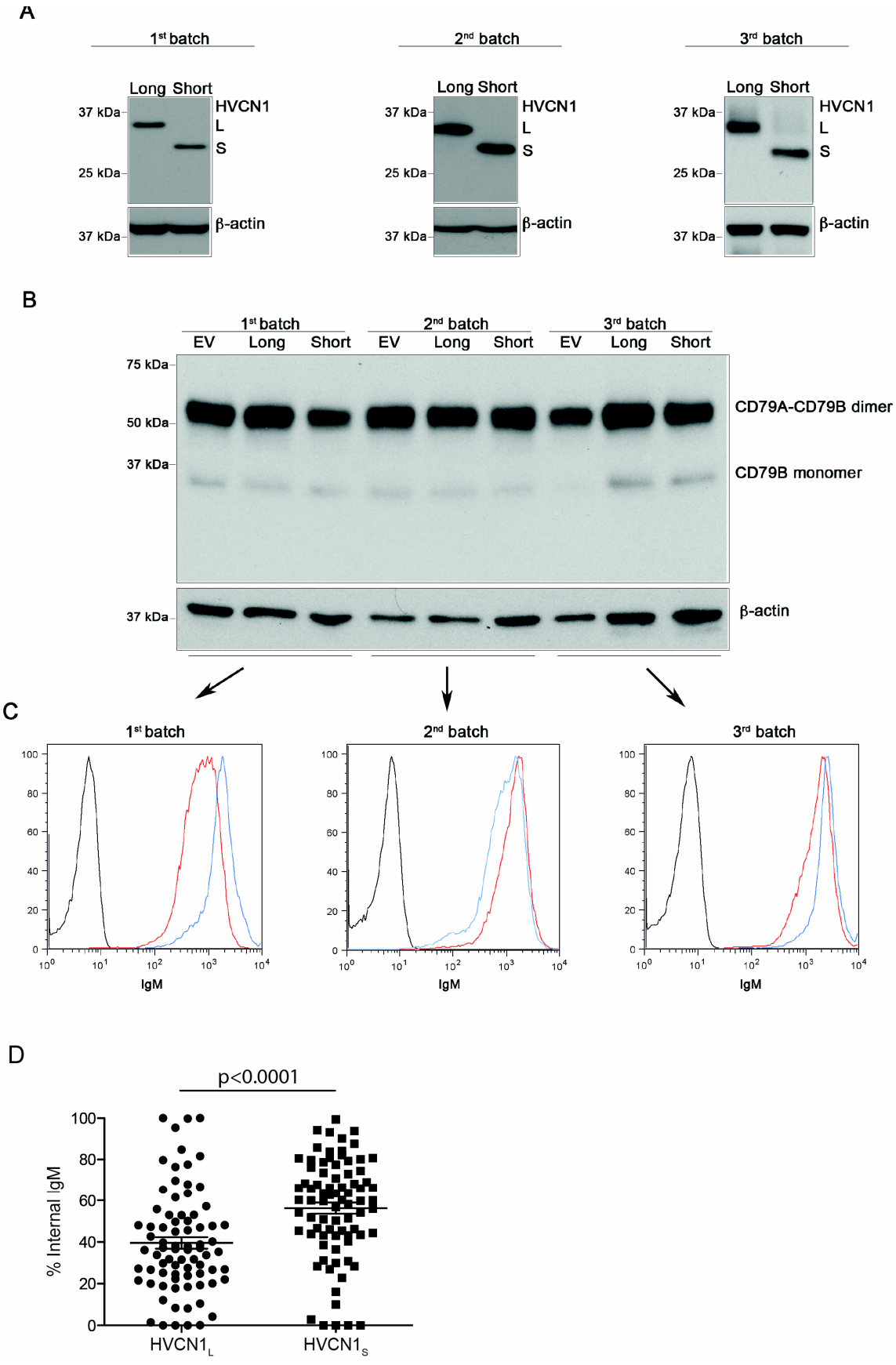
A
1st batch
2nd batch
3rd batch
Long Short
37 kDa
25 kDa
HVCN1
L
S
β-actin
B
1st batch
2nd batch
3rd batch
EV Long Short EV Long Short EV Long Short
75 kDa
50 kDa
37 kDa
CD79A-CD79B dimer
CD79B monomer
β-actin
C
1st batch
2nd batch
3rd batch
IgM
D
p<0.0001
% Internal IgM
HVCN1L
HVCN1S

Fig. S7. Levels of expression of HVCN1 and BCR complex components in A20 cell line overexpressing $HVCN1_L$ or $HVCN1_S$.

Three different batches of A20 cells were transduced with an empty vector (EV), $HVCN1_L$ (Long) or $HVCN1_S$ (Short). A) Immunoblot analysis showing $HVCN1_L$ (L) and $HVCN1_S$ (S) expression. β-actin was used as a loading control. B) Immunoblot of CD79B (immunoglobulin-associated-β or Ig-β), analyzed in non-reducing conditions. C) Flow cytometry analysis of IgM expression in the three different batches of cells. Blue histogram represents cells overexpressing $HVCN1_L$, red histogram cells overexpressing $HVCN1_S$ and black histogram unstained cells. D) Quantification of percentage of internalized IgM over total IgM in each cell. Each symbol represents a single cell (*n* = 78) and horizontal lines indicate the mean.

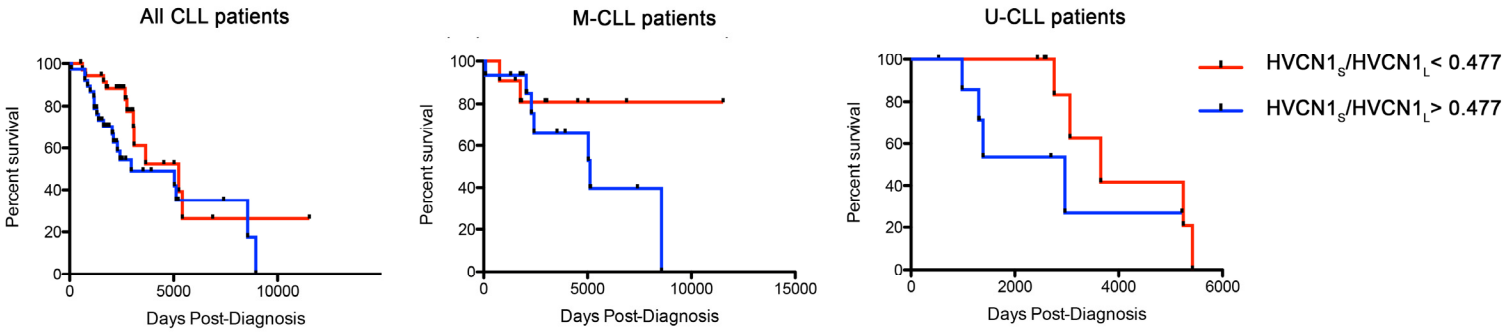

Fig. S8. CLL patients with higher expression of $HVCN1_S$ show a trend for reduced overall survival. *Left*) Kaplan-Meier curve for patients classified into either 'high' or 'low' for their ratio of $HVCN1_S$ expression over $HVCN1_L$ (red line = low $HVCN1_S$, blue line = high $HVCN1_S$), using the median ratio of 0.477 as a cut-off (Mantel-Cox $p = 0.0700$; red line $n = 36$, blue line $n = 38$). Levels of expression of $HVCN1_L$ and $HVCN1_S$ were determined by densitometry analysis of CLL protein lysates immunoblots, relative to loading control (α-tubulin) and normalized to a positive control used across different blots (cell line HBL1). (*Middle*) Kaplan-Meier curve for mutated (M-CLL) patients, classified as before ($p = 0.2747$; red line $n = 11$, blue line $n = 15$). (*Right*) Kaplan-Meier curve for unmutated (U-CLL) patients ($p = 0.1312$; red line $n = 10$, blue line $n = 7$).

Table S1. Gating kinetics of unstimulated LK35.2 cells with $HVCN1_S$, $HVCN1_L$, and $HVCN1_S$ mutants.

Construct	τ_{act} +60 mV (s)	τ_{tail} (ms)	$V_{threshold}$ (mV)
$HVCN1_S$	5.58 ± 1.13 (17)	370 ± 43 (19)	21.0 ± 2.2 (18)
$HVCN1_L$	* **2.24** ± 0.36 (10)	494 ± 88 (9)	15.6 ± 2.8 (11)
T9A	* **0.62** ± 0.076 (6)	453 ± 46 (8)	§ **-2.6** ± 3.6 (9)
S77A	3.91 ± 0.87 (8)	538 ± 83 (8)	* **12.0** ± 2.8 (8)
T9A/S77A	1.40 ± 0.82 (3)	399 ± 71 (5)	9.8 ± 6.5 (4)
T29A	‡ **0.51** ± 0.12 (5)	* **871** ± 59 (5)	§ **-12** ± 2.2 (5)
T29D	* **0.91** ± 0.44 (7)	508 ± 145 (8)	* **3.1** ± 3.5 (8)
S97A	2.14 ± 0.35 (6)	608 ± 79 (6)	19.5 ± 1.5 (6)
S97D	§ **0.77** ± 0.07 (25)	427 ± 53 (25)	12.6 ± 1.3 (25)
T29A/S97A	* **0.55** ± 0.11 (8)	* **848** ± 128 (8)	† **-3.8** ± 2.6 (8)

All cells were unstimulated and studied at pH_o = pH_i = 7.0 in perforated-patch configuration. Mean ± SEM (*n*) are given. Statistical differences from $HVCN1_S$ are indicated: * $p < 0.05$, ‡ $p < 0.01$, † $p < 0.001$, § $p < 0.0001$. The final five rows display data re-analyzed from a previous study of full–length HVCN1 expressed in LK35.2 cells (14). These values are compared statistically with $HVCN1_L$.

Table S2. Enhanced gating of $HVCN1_S$ with the S77A mutation in response to PMA or GFX.

S77A	τ_{act}		τ_{tail}		$g_{H,max}$		$V_{threshold}$	
	PMA	GFX	PMA	GFX	PMA	GFX	PMA	GFX
mean	2.34	3.20	1.31	1.26	1.86	2.38	14.0	7.5
SEM	0.47	0.89	0.12	0.16	0.25	0.66	2.4	2.5
n	6	4	6	4	6	4	5	4

Relative changes in each parameter are given (*i.e.*, 1.0 means no response). As in Fig. S5, the ratio for τ_{act} is (control/PMA), for τ_{tail} is (PMA/control), for $g_{H,max}$ is (control/PMA). For GFX reversal, the ratio for τ_{act} is (GFX/PMA), for τ_{tail} is (PMA/GFX), for $g_{H,max}$ is (GFX/PMA). $V_{threshold}$ values are the absolute magnitude of the negative shift produced by PMA and the positive shift produced by GFX. None of the responses differs significantly from $HVCN1_S$ responses, except for the GFX reversal of $V_{threshold}$, which was smaller for S77A.

Table S3. Characteristics of CLL Patients

			Clinical Data		Relative Expression of HVCN1				PKC	
Patient	Age	Sex	IGHV status	Survival (days)	$HVCN1_L$	$HVCN1_S$	Total	$HVCN1_S$/ $HVCN1_L$	Densitometry	+/-
B43	59	F		1632	2.9	1.6	4.5	0.5419	1.07994164	POS
B44	59	M		860	5	1.7	6.6	0.3376	0.929444745	POS
B45	88	F	M	85	2.9	1.3	4.2	0.4569	0.901620176	POS
B46	56	M		3073	5.5	3	8.5	0.5406	1.31332919	POS
B47	72	M	M	2953	2.5	0.9	3.4	0.3572	1.076176429	POS
B48	49	F		2807	5.6	3.2	8.8	0.5683	1.626910029	POS
B49	64	M		2710	5.5	2.7	8.2	0.4793	0.222747969	POS
B50	52	F		1160	15.7	12.8	28.6	0.8136	0.0754465	POS
B51	59	M		2527	3.5	2.1	5.6	0.6124	3.464993641	POS
B52	58	M		613	3.5	2.6	6	0.7521	0.506721317	POS
B53	66	F		8954	1.5	0.9	2.4	0.6174	0.153058909	POS
B54	75	F		2465	2.5	0.9	3.3	0.3421	0	NEG
B55	71	M		2345	2.2	3	5.2	1.3896	1.111757534	POS
B56	56	M		2437	1.3	1	2.3	0.7671	0	NEG
B57	80	F		2248	2.6	1.7	4.3	0.6659	2.631743971	POS
B58	56	M		3096	4.8	2.2	7	0.4585	0.082274197	POS
B59	82	M		1181	8.7	2.3	11	0.2689	0.972955833	POS
B60	87	M		726	3.6	1.6	5.2	0.4472	0.501670808	POS
B61	80	F		2248	8.7	3.5	12.2	0.4014	2.967775025	POS
B62	80	M	M	1758	3.9	1.4	5.3	0.3625	0.326367277	POS
B63	60	M		1788	9.3	2	11.3	0.2142	0.017556817	POS
B64	62	M		1706	15.8	3.3	19.1	0.2121	0.491560204	POS
B65	80	M		1858	10.5	5.4	15.8	0.5124	0.964239249	POS
B66	74	M		2673	6.9	1	7.9	0.1456	0.113335339	POS
B67	58	F		1553	19	3.8	22.9	0.2017	0	NEG
B68	82	M		1181	3.5	0.9	4.4	0.2499	1.474164936	POS
B69	74	M		2107	3.1	0.2	3.3	0.0628	0.59021759	POS
B70	83	M		1766	2.6	0.7	3.3	0.2613	1.086449383	POS
B71	60	M		2253	6.3	3	9.3	0.4761	0.308741844	POS
B72	54	M		1429	4.6	1.4	6	0.305	0.556051426	POS
B73	87	M		726	3.8	1.4	5.2	0.3566	1.945860305	POS
B74	79	M		2376	4.4	1.4	5.8	0.3204	0.089141168	POS
B75	63	F		2260	1	0.3	1.2	0.2651	1.496196771	POS
B76	59	F		1632	9	4.5	13.5	0.5046	1.936510285	POS
L1	68	m	U	2757	12.3	4	16.2	0.3222	0.48418262	POS
L10	52	m	U	2568	15.6	6.8	22.5	0.4375	0.016663283	POS
L11	65	m	M		24.4	14	38.4	0.5757	0	NEG
L12	66	m	U	1389	18.1	10.7	28.8	0.5904	0.460398151	POS
L13	76	f	U	2434	16.7	0.7	17.4	0.0389	0	NEG

L14	78	f	M	2042	4.8	1.7	6.5	0.3615	0.849684093	POS
L15	52	m	U	5219	15.8	5.7	21.5	0.3574	0.807601688	POS
L16	59	m	M	7403	3.6	0.7	4.3	0.2083	0.902562487	POS
L17	58	m	U	1315	8.8	5.9	14.8	0.6697	1.335926487	POS
L18	60	f	M	1299	15	11.2	26.3	0.7448	0	NEG
L19	84	f	U	984	5.6	0.8	6.3	0.1388	0	NEG
L2	62	f	M	2296	17.7	10.9	28.6	0.6162	0	NEG
L20	53	m	U	5420	137.8	77.4	164.1	0.5613	1.301714473	POS
L21	68	f	M	3917	40.4	19.1	45.4	0.4734	0	NEG
L22	76	m	M	2418	11.6	13.5	19.2	1.1663	0.153943666	POS
L23	61	m	M	2068	26.9	30.4	43.7	1.1291	0.210359159	POS
L24	78	f	M	1819	144.6	39	140	0.2693	0.035721496	POS
L25	59	m	U	5246	25.9	20.4	35.3	0.7874	0.346232682	POS
L26	65	m	M	1777	79.2	49.5	98.1	0.6248	0.264791187	POS
L27		f	U		9.6	5.9	15.5	0.6207	0.223836649	POS
L28	52	m	M	11525	4.6	1.8	6.4	0.3926	0.195476388	POS
L29	57	f	M	6883	5.6	3.3	8.9	0.5879	0.411740779	POS
L3	78	m	U	1305	9.3	6.2	15.5	0.6674	0.094403426	POS
L30	60	f	U	2603	6.7	4.9	11.6	0.7283	1.720449536	POS
L31	62	m	M	5148	4.4	2.6	7	0.5815	0.945405162	POS
L32	56	m	M	1518	6.3	2.5	8.9	0.4018	0.783520755	POS
L33	47	m	U	3060	4.5	1.8	6.2	0.394	0.821684589	POS
L34	76	m	M	3037	3.3	2.9	6.2	0.8745	0.335089518	POS
L35	58	m	M	4526	5.5	2.6	8.1	0.4739	0.252284566	POS
L36	54	m	U	532	6.6	5.3	11.9	0.8019	0.054676042	POS
L37	55	f	M	5022	6.4	4.6	11	0.7261	0.322348723	POS
L38	68	m	M	1760	2.3	4.5	6.8	1.9503	0.791368449	POS
L39	80	m	M	763	12	9.1	21.1	0.7548	0.768639263	POS
L4	62	f	U	2966	5.1	1.8	6.9	0.3455	0.612410555	POS
L40	59	m	U	3656	81	39.1	120.1	0.4824	0	NEG
L41	77	f	U	2757	10.6	8.8	19.5	0.8304	0.149925269	POS
L42	56	m	U	2694	27.1	19.8	46.9	0.7293	0.583203639	POS
L5	76	m	M	5038	4.6	1.5	6.1	0.318	0.017601259	POS
L6	58	m	M	1896	10	2.1	12	0.2095	0.088580175	POS
L7	66	f	M	8566	4.2	1.3	5.5	0.3075	0.212741553	POS
L8	52	f	M	5119	3.5	2.2	5.7	0.6417	0.468254735	POS
L9	64	m	M	3527	22	10.9	33	0.4951	0	NEG

IGHV status: mutation status of the immunoglobulin variable heavy chain variable region at the time of sampling; either mutated (M) or unmutated (U). Survival: time in days between diagnosis and death or database last update.

HVCN1 and PKC protein expression levels as determined by western blot, relative to loading control (α-tubulin) and normalized to positive control (HBL1 lysate). PKC expression considered positive (Pos) if greater than 0 or negative (Neg) if equal to 0. Samples were collected from patients evaluated at St Bartholomew's (London) and Leicester Royal Infirmary hospitals after they provided written informed consent, in accordance with the Declaration of Helsinki.

Supporting Materials and Methods

Gradient PCR

HBL1 cells were lysed using QIAshredder spin columns (Qiagen; 79656), total RNA extracted using RNeasy Mini Kit (Qiagen; 74106) and genomic DNA degraded with RNase-free DNase Set (Qiagen; 79254). cDNA was then synthesized using High Capacity cDNA Reverse Transcription Kit (Applied Biosystems; 4368814) all according to the manufacturer's instructions.

Gradient PCR reactions with annealing temperatures ranging from 49-72°C were carried out for 35 cycles on a Tetrad PTC-225 Thermal Cycler (MJ Research).

Pfx50™ DNA Polymerase (Invitrogen; 12355-012) was used according to manufacturers instructions with 0.3 mM dNTPs (Qiagen; 201913) and 2 μl of cDNA template. The reverse primer used for all pairs was 5′-CTCAACATGCCCCTGAAGTC-3′. The forward primer to recognize all 3 variants: 5′-CGCTGAGAGGATGAGCAAGT-3′; variant 2: 5′-TGCTCTGAGGCTCCCAGT-3′; variants 1 and 3: 5′-GTACGAGTTGGCCCGGAG-3′. All primers synthesized by Sigma Aldrich.

Reaction products were run on 2% agarose gels supplemented with 10% GelRed Nucleic Acid Gel Stain (Biotium; 41003) and HyperLadder IV (Bioline; BIO-33056) for DNA molecular weight markers.

Retroviral production and cell transduction

Retroviral particles were produced in Phoenix α packaging cells. Cells were transfected with MigRI empty vector and HVCN1 constructs (See materials & methods) by Ca^{2+} phosphate. Viral supernatants were collected after 24, 36 and 48 h.

A20 D1.3 and LK35.2 HyHEL10 cell lines were transduced by spinoculation at 2300 rpm for 90 min in the presence of 4 μg/ml Polybrene (Sigma Aldrich), three times over a period of 2 days.

Co-Immunoprecipitation assay

A20 D1.3 cells overexpressing $HVCN1_L$ or $HVCN1_S$ were lysed for 30 min in 20 mM Hepes, 1% CHAPS (3-[(3-Cholamidopropyl)-dimethylammonio]-1-propanesulfonate hydrate), 137 mM NaCl, 2 mM EDTA and proteases inhibitors (Sigma Aldrich). After

centrifuging the lysate at 12,000g for 10 minutes to sediment cell debris, supernatants were cleared with Protein G Sepharose beads (GE Healthcare). Immunoprecipitation was carried out using 1 mg anti-myc tag antibody (9B11; Cell Signaling Technology), or anti-CD79B (or immunoglobulin-associated-β; AT107-2; Serotec) conjugated to Protein G Sepharose beads. An equal amount of Protein-G beads conjugated to mouse or rat IgG were used as negative control. After washing with lysis buffer, beads were resuspended in 2x Laemmli sample buffer without β-mercaptoethanol (non-reducing conditions) and analyzed by western blot.

Immunofluorescence Microscopy

A20 D1.3 cells were stimulated with APC-conjugated $F(ab')_2$ anti-IgM (Jackson Laboratories) at 37°C for 30 min, washed with PBS and added to poly-L-lysine coated glass slides. Cells were then fixed in 4% paraformaldehyde for 20 min, washed three times with 0.1% saponin in PBS and blocked with 5% goat serum, 0.1% saponin in PBS for 10 min before being incubated overnight at 4°C in a humid chamber with AlexaFluor555-conjugated anti-myc (Cell Signaling; 9B11) in PBS with 5% goat serum and 0.1% saponin. Cells were subsequently washed twice, incubated with DAPI for 5 min, washed a final time and mounted with glass coverslips with ProLong® Gold Antifade Mountant (Life Technologies; P36930).

Slides were visualized using the Zeiss LSM 510 Meta Confocal Microscope.

Western Blot

Cell samples were lysed in SDS sample buffer (0.5M Tris-HCl pH 6.8, 20% glycerol, 4% SDS, 2% β-mercaptoethanol, ddH_2O and bromphenol blue) and sonicated for 10 s pulses, three times.

Proteins were separated by electrophoresis in 10% Mini-PROTEAN® TGX™ Gels (BioRad; 456-1034) at 90V and subsequently transferred to PVDF membranes (Perkin Elmer) by wet transfer.

Membranes were blocked with 5% Milk Powder in PBS for 45 min then incubated with either rabbit anti-HVCN1 (CovalAb), rabbit anti-phospho-PKC (pan) (Cell Signaling; 9371S), rabbit anti-phospho-p44/42 MAPK (Erk) (Cell Signaling; D13.14.4E), mouse

anti-p44/42 MAPK (Cell Signaling; 4696), mouse anti-β-actin (Cell Signaling; 4970) or mouse anti-α-tubulin (eBiosciences; 14-4502-82), either overnight at 4°C or 1 h at room temperature. Membranes were subsequently washed three times with PBST (0.05%TWEEN in PBS) before incubation for 1 h at room temperature with either HRP-conjugated anti-rabbit or –mouse (GE Healthcare; NA9340V – NXA931), as appropriate. Finally, they were washed a further three times with PBST before being covered with the chemiluminescence agent, ECL (GE Healthcare; RPN2106) and exposed to X-ray film (Fuji Film; 4741019236).
Densitometry was performed using ImageJ 1.45s software.

Migration assay

$3x10^5$ A20 D1.3 overexpressing EV, $HVCN1_L$ or $HVCN1_S$ were seeded onto transwell inserts with 5 μm pore size polycarbonate membranes (Corning), and either media or media containing 100ng/ml CXCL12 was added in the bottom of the well. Cells migrated into the well were re-suspended and their number determined by counting on a haemocytometer after 4h.

Proliferation assay

Cell proliferation was determined using the Click-iT Edu Imaging Kit (Invitrogen), according to the manufacturer's instructions. $5x10^5$ cells were incubated with 5 μM 5-ethynyl-2'-deoxyuridine (Edu) for 3h at 37°C. Subsequently, cells were fixed with 3.7 % formaldehyde for 15 min and permeabilized with 0.5 % Triton X-100 for 20 min. Immunofluorescent staining was carried out by incubation with anti-GFP, chicken IgY antibody (Invitrogen; A10262) for 1h. After two washes, cells were incubated with the Click-iT reaction cocktail for 30 minutes, in the dark. Finally, cells were incubated with Alexa Fluor 488 goat anti-chicken antibody (Invitrogen; A11039) for 40 minutes. Nuclei were stained with DAPI, and cells mounted with glass coverslips with ProLong® Gold Antifade mounting solution (Life Technologies). Cells were visualized using Zeiss LSM 510 Meta Confocal Microscope.

Supporting Information References

1. Bánfi B, et al. (1999) A novel H^+ conductance in eosinophils: unique characteristics and absence in chronic granulomatous disease. *J Exp Med* 190(2):183-94.
2. DeCoursey TE, Cherny VV, DeCoursey AG, Xu W, Thomas LL (2001) Interactions between NADPH oxidase-related proton and electron currents in human eosinophils. *J Physiol* 535(Pt 3):767-81.
3. DeCoursey TE, Cherny VV, Zhou W, Thomas LL (2000) Simultaneous activation of NADPH oxidase-related proton and electron currents in human neutrophils. *Proc Natl Acad Sci USA* 97(12):6885-9.
4. Lishko PV, Botchkina IL, Fedorenko A, Kirichok Y (2010) Acid extrusion from human spermatozoa is mediated by flagellar voltage-gated proton channel. *Cell* 140(3):327-337.
5. Morgan D, et al. (2007) Sustained activation of proton channels and NADPH oxidase in human eosinophils and murine granulocytes requires PKC but not $cPLA_2\alpha$ activity. *J Physiol* 579(Pt 2):327-44.
6. Mori H, et al. (2003) Regulatory mechanisms and physiological relevance of a voltage-gated H^+ channel in murine osteoclasts: phorbol myristate acetate induces cell acidosis and the channel activation. *J Bone Miner Res* 18(11):2069-76.
7. Musset B, Cherny VV, DeCoursey TE (2012) Strong glucose dependence of electron current in human monocytes. *Am J Physiol Cell Physiol* 302:C286-C295.
8. Musset B, et al. (2008) A pH-stabilizing role of voltage-gated proton channels in IgE-mediated activation of human basophils. *Proc Natl Acad Sci USA* 105(31):11020-11025.
9. DeCoursey TE (2010) Voltage-gated proton channels find their dream job managing the respiratory burst in phagocytes. *Physiology (Bethesda)* 25(1):27-40.
10. Cherny VV, Henderson LM, Xu W, Thomas LL, DeCoursey TE (2001) Activation of NADPH oxidase-related proton and electron currents in human eosinophils by arachidonic acid. *J Physiol* 535(Pt 3):783-94.
11. DeCoursey TE, Cherny VV, Morgan D, Katz BZ, Dinauer MC (2001) The $gp91^{phox}$ component of NADPH oxidase is not the voltage-gated proton channel in phagocytes, but it helps. *J Biol Chem* 276(39):36063-6.
12. Szteyn K, Yang W, Schmid E, Lang F, Shumilina E (2012) Lipopolysaccharide-sensitive H^+ current in dendritic cells. *Am J Physiol Cell Physiol* 303(2):C204-12.
13. Musset B, Cherny VV, Morgan D, DeCoursey TE (2009) The intimate and mysterious relationship between proton channels and NADPH oxidase. *FEBS Lett* 583(1):7-12.
14. Musset B, et al. (2010) Identification of Thr^{29} as a critical phosphorylation site that activates the human proton channel *Hvcn1* in leukocytes. *J Biol Chem* 285(8):5117-21.